An anthraquinone-based bismuth-iron Metal-Organic Framework as efficient photoanode in photoelectrochemical cells

Cai Shi,[a] Miguel Gomez-Mendoza,[b] Eloy Gómez de Oliveira,[a] Miguel García-Tecedor,[b] Mariam Barawi,[b] Fátima Esteban-Betegón,[a] Marta Liras,[b] Enrique Gutiérrez-Puebla,[a] Angeles Monge,[a] Víctor A. de la Peña O'Shea*[b] and Felipe Gándara*[a]

a Dr. C. Shi, Mr. E. Gómez de Olveira, Dr. F. Esteban, Prof. E. Gutiérrez-Puebla, Prof. A. Monge, Dr. F. Gándara
Materials Science Institute of Madrid – Spanish National Research Council,
Sor Juana Inés de la Cruz, 3, 28049, Madrid, Spain
E-mail: gandara@icmm.csic.es, victordelapenya@imdea.org

b Dr. M. Barawi, Dr. M. Gomez-Mendoza, Dr. M. García-Tecedor, Dr. M. Liras, Prof. V. A. de la Peña-O'Shea
[2]Photoactivated Processes Unit
IMDEA Energy Institute
Móstoles Technology Park, Avenida Ramón de la Sagra 3, Móstoles, 28935, Madrid, Spain

Electronic Supporting Information

Table of contents

Experimental and computational details

Fig. S12 A) Transient absorption spectra (λ_{exc} = 355 nm) at different timescales and C) comparative of the normalized transient decay traces after laser excitation at λ_{exc} = 355 nm (λ_{mon} = 388 and 480 nm) for 2, 6-AQDS, BiPF-10, and BiFePF-15 in water under N_2. B) 2D mapping transient absorption spectra of BiFePF-15 in water under N_2.

Fig. S13 A) Transient absorption spectra (λ_{exc} = 355 nm) for 2, 6-AQDS ligand in the presence of 0.5 M Na_2SO_3 in deaerated aqueous solution at different timescales. B) Comparative of the transient absorption spectrum for 2, 6-AQDS ligand in absence or presence of 0.5 M Na_2SO_3 immediately after laser pulse 0 μs or upon 30 μs. The signal for 0.5 M Na_2SO_3 is included for comparison. C and D) Transient decay traces (λ_{exc} = 355 nm) for 2, 6-AQDS ligand monitored at (C) λ_{mon} = 385 nm or (D) λ_{mon} = 480 nm, respectively. The fitting curves (blue) have been included in all cases.

Fig. S14 A) Transient absorption spectra (λ_{exc} = 355 nm) for BiPF-10 MOF in the presence of 0.5 M Na_2SO_3 in aqueous solution suspension at different timescales under N_2. B) Comparative of the transient absorption spectrum for BiPF-10 MOF in absence or presence of 0.5 M Na_2SO_3 immediately after laser pulse 0 μs or upon 30 μs. The signal for 0.5 M Na_2SO_3 is included for comparison. C and D) Transient decay traces (λ_{exc} = 355 nm) for BiPF-10 MOF monitored at (C) λ_{mon} = 385 nm or (D) λ_{mon} = 480 nm, respectively. The fitting curves (blue) have been included in all cases.

Fig. S15 A) Transient absorption spectra (λ_{exc} = 355 nm) for BiFePF-15 MOF in the presence of 0.5 M Na_2SO_3 in aqueous solution suspension at different timescales under N_2. B) Comparative of the transient absorption spectrum for BiFePF-15 MOF in absence or presence of 0.5 M Na_2SO_3 immediately after laser pulse 0 μs or upon 30 μs. The signal for 0.5 M Na_2SO_3 is included for comparison. C and D) Transient decay traces (λ_{exc} = 355 nm) for BiFePF-15 MOF monitored at (C) λ_{mon} = 385 nm or (D) λ_{mon} = 480 nm, respectively. The fitting curves (blue) have been included in all cases.

Fig. S16 Comparative of the transient decay traces (A) and normalized (B) after laser excitation at λ_{exc} = 355 nm (λ_{mon} = 520 nm) for 2, 6-AQDS ligand and BiPF-10 and BiFePF-15 MOFs in the presence of aqueous Na_2SO_3 0.5 M under N_2.

Fig. S17 Comparative transient absorption spectra (exc = 355 nm) for A) 2, 6-AQDS, B) BiPF-10 and C) BiFePF-15 in the presence of 0.5 M Na_2SO_3 in aqueous solution suspension at different timescales under N_2.

Fig. S18 UV–Vis spectra of BiFePF-15 and TD-DFT (6-31G**) calculated excitation energies (vertical bars) and selected molecular orbitals contributing to ligand metal charge transfer transitions.

Table S3 Summary of bare MOFs as photo-electrocatalyst for H_2 production in reported publications.

References.

.

Experimental details

MOF Synthesis. The two new materials were synthesized by microwave-assisted heating and conventional hydrothermal heating. BiPF-10 was prepared under microwave assisted heating (Microwave Synthesizer, Discover®, CEM Corporation, US). $Bi(NO_3)_3 \cdot 5H_2O$ (0.100 g, 0.2 mmol, from Alfa Aesar, 98% purity), and 2, 6-AQDS (0.086 g, 0.2 mmol, Fluka, HPLC grade) were dissolved in 3.7 mL of distilled water and 300 µL methylsulfonic acid (CH_3SO_3H, Fluka). The mixture was heated at 180 °C for 1 h, under stirring, with 260 psi of pressure and 200 W power, after cooling to room temperature, yellow, sheet-like crystals were obtained, centrifuged and consecutively washed with 10 mL of water, ethanol, and acetone. BiFePF-15 was synthesized by dissolving $Bi(NO_3)_3 \cdot 5H_2O$ (0.097 g, 0.2 mmol), $Fe(NO_3)_3 \cdot 9H_2O$ (0.081 g, 0.2 mmol, Alfa Aesar, 98% purity), and 2, 6-AQDS disodium salt (0.083 g, 0.2 mmol) in 10 mL of distilled water and 200 µL of concentrated nitric acid (HNO_3, Scharlau). The solution was transferred to a Teflon-lined steel autoclave and heated at 150 °C for 48 h in a pre-heated oven. After cooling down to room temperature, orange, sheet shaped crystals were isolated by centrifugation and consecutively washed with 10 mL of water, ethanol, and acetone.

Single Crystal X-ray Diffraction. Crystals were selected with a polarized optical microscope for a single crystal X-ray diffraction experiment. Single crystal X-ray data were collected in Bruker four circle κ-diffractometer equipped with a Cu INCOATED microsource, operated at 30 W power (45 kV, 0.60 mA) to generate Cu Kα radiation (λ = 1.54178 Å), and a Bruker Photon III area detector. Diffraction data were collected exploring over the reciprocal space in a combination of φ and ω scans to reach a resolution of 0.85 Å, with a completeness > 95%, and redundancy > 3. For this, either a generic quadrant collection strategy or a specific one determined using Bruker APEX4 software suite was used. The exposure time was adjusted based on the size and diffracting quality of the specimens, each exposure covering 1° in ω or φ. Unit cell dimensions were determined for least-squares fit of reflections with $I > 4\sigma$. The structures were solved by intrinsic phasing or direct methods, implemented in SHELX package. The hydrogen atoms were fixed at their calculated positions using distances and angle constraints. All calculations were performed using APEX4 software for data collection and OLEX2 and SHELXTL22 to resolve and refine the structure. All non-hydrogen atoms were anisotropically refined.

Powder X-ray Diffraction. Powder X-ray diffraction (PXRD) patterns were measured with a Bruker D8 diffractometer with a copper source operated at 1600 W, with step size = 0.02° and exposure time = 0.5 s/step from 4° to 50°.

Ultraviolet-Visible Diffuse Reflectance Spectroscopy. Ultraviolet–visible diffuse reflectance spectra (UV–vis DRS) of the solid powdered samples were obtained in a Perkin Elmer Lambda 1050 UV/Vis/NIR. The experiments were performed in the range of 250-700 nm.

Photoluminescence. Photoluminescence experiments of solid samples (2, 6-AQDS, BiPF-10 and BiFePF-15) were carried out with a Fluorescence Spectrometer Perkin Elmer LS 55, with an excitation wavelength of 372 nm and using a cut-off filter at 430 nm in front face mode. The experiments were carried out in the range of 382-900 nm.

Time-Resolved Photoluminescence Spectroscopy. Decay curves of solid 2, 6-AQDS, BiPF-10, and BiFePF-15 were performed with Edinburgh Instruments Mini-τ (EPL-375). According to the photoluminescence emission spectrum of BiFePF-15, we chose an excitation wavelength of 372 nm, and detected thought band-pass filter in the range between 425-475 nm. The photoluminescence lifetimes were fitted by the decay curves, and calculated by *Equation 1*:

$$< \boldsymbol{\tau} >= \{\sum(\boldsymbol{A_i\tau_i})^2\}/\sum(\boldsymbol{A_i\tau_i}) \qquad \textit{Equation 1}$$

Transient Absorption Spectroscopy (TAS) Measurements. Experiments were performed using a laser flash photolysis LP980 equipment from Edinburgh Instruments (LP980), based on an optical parametric oscillator (OPO) pumped by the third harmonic of a Nd:YAG laser (EKSPLA). The selected excitation wavelength for the measurements was 355 nm with single low energy pulses of 1 mJ per pulse of ≈ 5 ns duration, while a pulsed xenon flash lamp (150 W) was employed as detecting light source. The probe light is dispersed through a monochromator (TMS302-A, grating 150 lines mm^{-1}) after it has passed the sample and then reaches a PMT detector (Hamamatsu Photonics) to obtain the temporal profile. The absorbance of all samples was kept at ≈0.3 at λ_{exc} = 355 nm as dispersed aqueous solutions. Measurements were conducted in absence or presence of 0.5 M Na_2SO_3 as sacrificial agent to simulate the reaction media in photocatalytic H_2 evolution studies. Since the measurements for BiPF-10 and BiFePF-15 MOFs were in aqueous dispersions, poor signal-noise was obtained at the detection limit of the transient between 300-400 nm, thus being the lifetime monitored at 520 nm more accurate (Figure S16). All transient spectra were recorded at room temperature using 10 × 10 mm^2 quartz cells, which were bubbled for 15 min with N_2 before acquisition.

Photoelectrochemical Measurements. Experiments were performed in a three-electrode glass cell with a quartz window containing 0.5 M sodium sulfite aqueous solution (Na_2SO_3, pH = 9) for photoelectrochemical and electrochemical measurements, respectively. Platinum wire was employed as counter electrode, while the reference was an Ag/AgCl electrode. The working electrode was prepared by dispersing MOF (8.5 mg) in isopropanol (1 mL) with 50 µL Nafion and depositing 30 µL of the suspension by drop-casting on fluorine doped tin oxide (FTO) cover glasses (1 cm × 1 cm). Voltage and current density (under dark and illumination condition) were recorded with a potentiostat-galvanostat PGSTAT204 provided with an integrated impedance module FRAII. A solar simulator (lot LSH302 Xe lamp and an LSZ389 AM1.5 global filter) was utilized as a light source.

For photoelectrochemical H_2 production experiments, 50 cm^3 STP min^{-1} of argon flow was passed through the Na_2SO_3 aqueous solution (0.5 M) during the reaction

to purge the system, also to act as a carrier gas. In this specific configuration, Na_2SO_3 is photoelectrocatalytically oxidized (acting as hole scavenger) in the BiFePF-15 electrode while H_2 is produced at Pt wire using the photogenerated electrons at the photoanode. The cell was connected to a gas chromatograph (Agilent micro-GC 490) equipped with a MS5A column with a temperature of 60 ºC and a TCD detector to quantify H_2.

Theoretical calculations. Periodic density functional theory (DFT) calculations for geometry and electronic structure were carried out using Viena ab initio simulation package (VASP). The total energies of the optimized geometries were estimated using the spin polarized version of the Perdew−Burke−Ernzerhof (PBE). A more accurate energy gap was fitted using the Heyd-Scuseria-Enzerhof hybrid functional (HSE06) with a mixing parameter of 0.25. A cut-off of 500 eV was set for the kinetic energy of the plane-waves to ensure a total energy and force convergence higher than 10^{-4} eV and 0.01 eV/Å^3, respectively. Optoelectronics properties of BiFePF-15 were calculated using Time dependent Density Functional Theory (TD-DFT) implemented in the software Gaussian 09 employing a PBE0 functional. The standard 6–31G(d.p) basis set of double split valence plus polarization functions also on H atoms was chosen. Moreover, a fix number of 500 states were selected for a proper comparison between all configurations and models.

Table S1 Crystal and structure refinement data for BiPF-10.

Identification code	BiPF-10
Empirical formula	$C_{14}H_8BiO_{10}S_2$
Formula weight	609.28
Temperature/K	250.0
Crystal system	triclinic
Space group	*P-1*
a/Å	5.5635(2)
b/Å	9.3426(3)
c/Å	15.4190(5)
α/°	98.5980(10)
β/°	96.2630(10)
γ/°	103.8970(10)
Volume/Å^3	760.41(4)
Z	2
ρ_{calc}g/cm^3	2.628
μ/mm^{-1}	25.917
F(000)	559.0
Crystal size/mm^3	0.05 × 0.05 × 0.03
Radiation	CuKα (λ = 1.54184)
2Θ range for data collection/°	9.918 to 130.404
Index ranges	-6 ≤ h ≤ 6, -10 ≤ k ≤ 10, -18 ≤ l ≤ 18
Reflections collected	10095
Independent reflections	2571 [R_{int} = 0.0397, R_{sigma} = 0.0321]
Data/restraints/parameters	2571/0/245
Goodness-of-fit on F^2	1.103
Final R indexes [I>=2σ (I)]	R_1 = 0.0230, wR_2 = 0.0679
Final R indexes [all data]	R_1 = 0.0238, wR_2 = 0.0686
Largest diff. peak/hole / e Å^{-3}	0.99/-2.35

Table S2 Crystal and structure refinement data for BiFePF-15.

Identification code	BiFePF-15
Empirical formula	$C_{28}H_{12}Bi_2Fe_2O_{23}S_4$
Formula weight	1374.28
Temperature/K	250.15
Crystal system	monoclinic
Space group	*C2/c*
a/Å	32.9343(14)
b/Å	6.5367(3)
c/Å	15.9709(7)
α/°	90
β/°	93.5630(10)
γ/°	90
Volume/Å^3	3431.6(3)
Z	4
ρ_{calc}g/cm^3	2.660
μ/mm^{-1}	29.607
F(000)	2584.0
Crystal size/mm^3	0.01 × 0.01 × 0.01
Radiation	CuKα (λ = 1.54178)
2Θ range for data collection/°	12.036 to 130.268
Index ranges	-38 ≤ h ≤ 38, -7 ≤ k ≤ 7, -17 ≤ l ≤ 18
Reflections collected	16185
Independent reflections	2926 [R_{int} = 0.0353, R_{sigma} = 0.0290]
Data/restraints/parameters	2926/0/264
Goodness-of-fit on F^2	1.103
Final R indexes [I>=2σ (I)]	R_1 = 0.0372, wR_2 = 0.0939
Final R indexes [all data]	R_1 = 0.0372, wR_2 = 0.0939
Largest diff. peak/hole / e Å^{-3}	4.93/-1.74

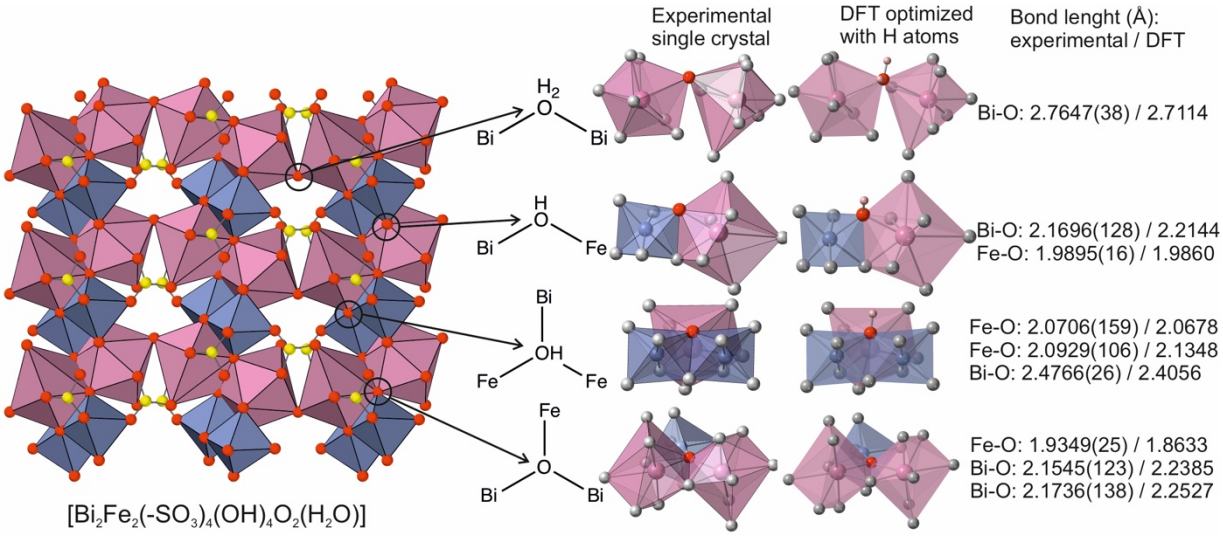

Fig. S1 Details of the location of hydrogen atoms in the inorganic SBU of BiFePF-15 through DFT based structural optimization.

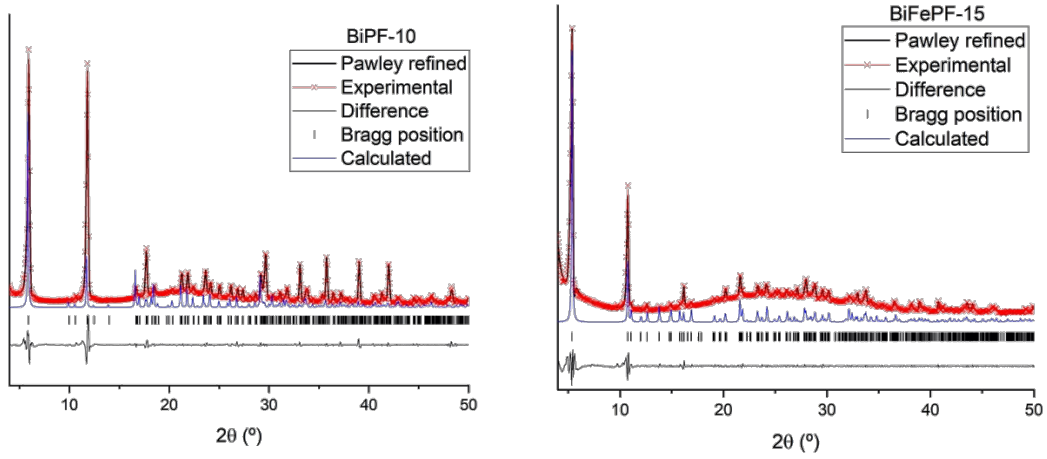

Fig. S2 Experimental and calculated PXRD patterns, and Pawley refined profiles for BiPF-10 (left) and BiFePF-15 (right).

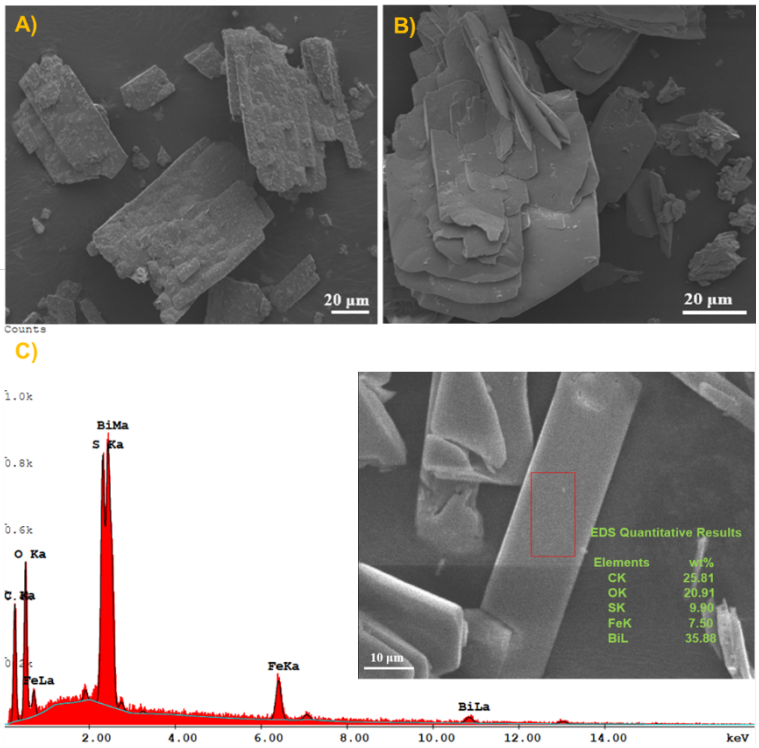

Fig. S3 SEM images of A) BiPF-10 and B) BiFePF-15; C) EDS results of BiFePF-15. The SEM images were taken with a FESEM FEI Nova NANOSEM 230 microscope under an operating voltage between 5-15 kV. The samples were synthesized by placing the crystals on a conductive carbon tape with double sides, attached to an aluminum sample holder, and later metallized with a layer of gold with13 nm thick with a Lecia EM ACE200 sputter. EDS microanalysis was conducted under 18 kV with an EDAX Apollo 10-300 mm detector. The points were recorded basically from the body and the basal plane of the crystal. Both BiPF-10 and BiFePF-15 exhibit similar two-dimensional layer shaped crystals (Fig. S3A and B). EDS results of BiFePF-15 demonstrate the presence of bismuth and iron in one crystal (Fig. S3C).

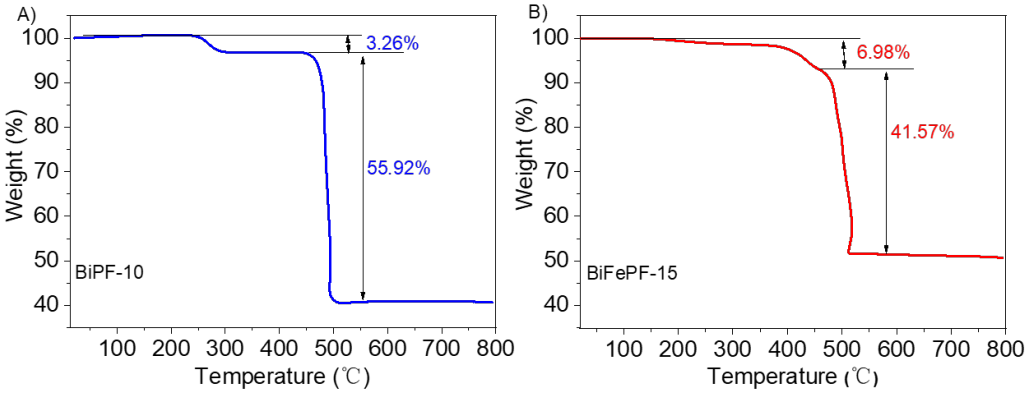

Fig. S4 Thermogravimetrical analysis of A) BiPF-10 and B) BiFePF-15 in air. Thermogravimetric experiments were performed in a SDT Q600 V20.9 Build 20 from TA Instruments with a heating rate of 10 ℃ min^{-1} between 25 and 800 ℃ under flowing air (100 mL min^{-1}). The experiment of BiPF-10 shows the mass loss of approximately 3.26% corresponding to the evaporation of water molecule, while the decomposition of the linker takes place at 493 ℃. For BiFePF-15, there is no obvious mass loss observed for water molecule. The main weight loss starts at about 400 ℃, until 520 ℃.

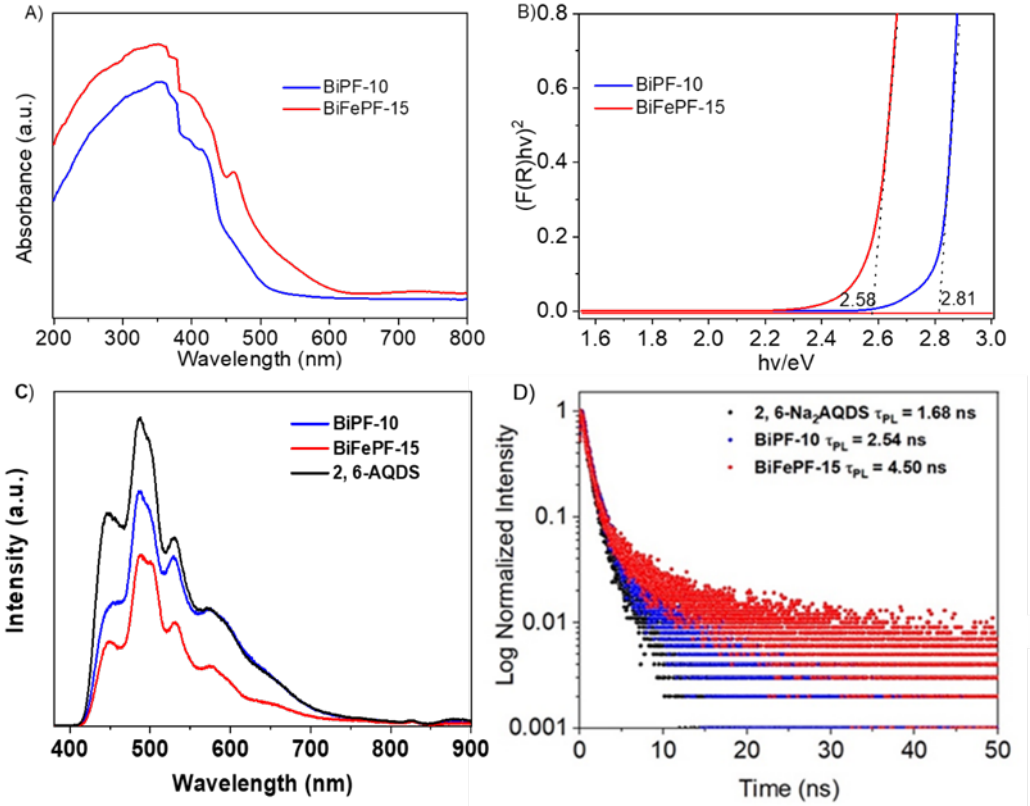

Fig. S5 A) UV-vis DRS spectra, B) tauc plots as direct transition for BiPF-10 and BiFePF-15, C) Photoluminescence spectra for 2, 6-AQDS and BiPF-10 and BiFePF-15, D) Time-resolved photoluminescence decay traces and corresponding calculated lifetime values.

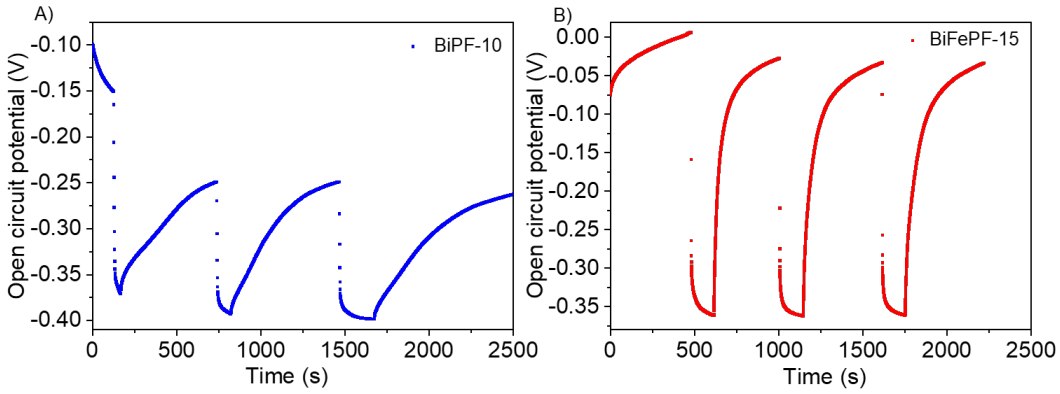

Fig. S6 Open circuit potential of A) BiPF-10 and B) BiFePF-15.

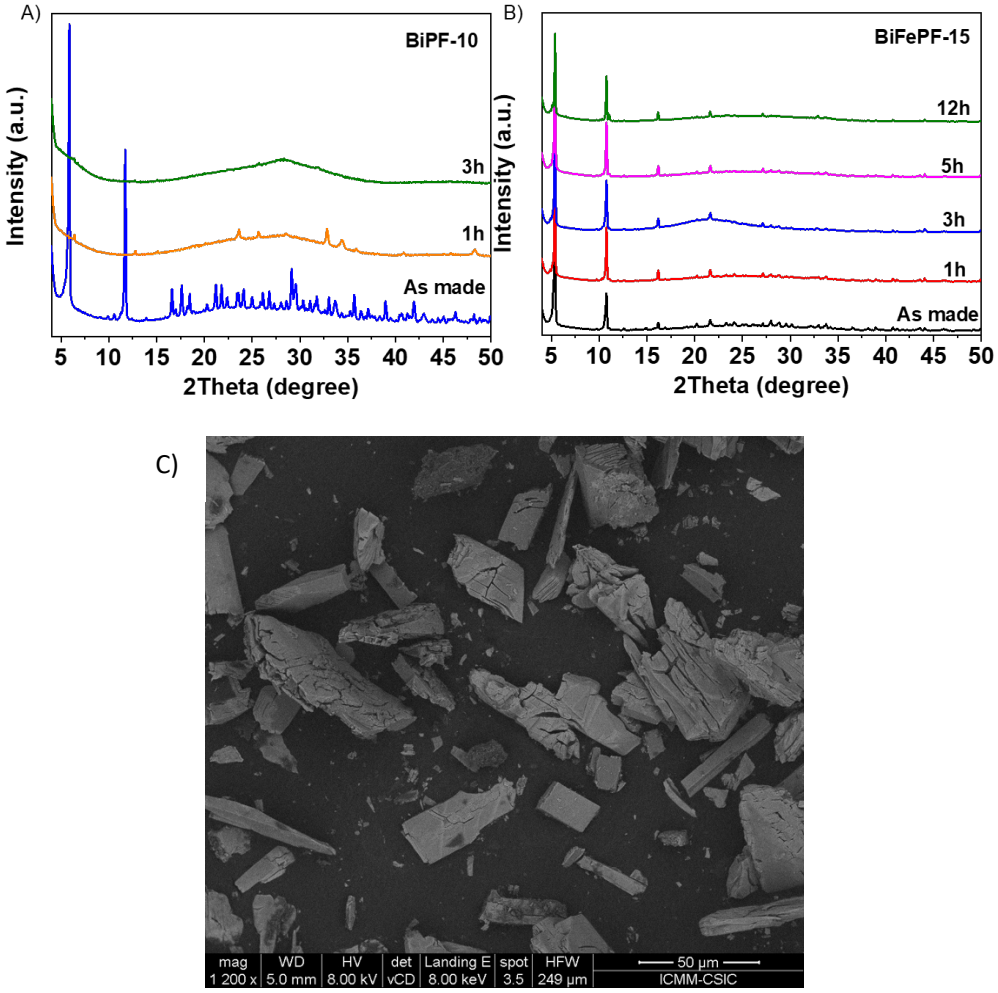

Fig. S7 PXRD patterns of A) BiPF-10, and B) BiFePF-15 before and after soaking in 0.5 M Na_2SO_3 aqueous solution. C) shows SEM image of crystals of BiFePF-15 after 2 h soaked in 0.5 M Na_2SO_3 aqueous solution

TAS Experiments of 2, 6-AQDS in Water. First, TAS experiments for the 2, 6-AQDS linker dissolved in water were performed. In the case of the aqueous photochemistry of sulphonated anthraquinones all possible reported mechanisms begin with reaction of the triplet due its high intersystem crossing yield (ϕ_{ISC}=ISC 0.91), takes 0.4 ps[1, 2] and a short-lived singlet.[3, 4] The transient absorption spectrum for 2, 6-AQDS was complex, where three species can be observed centered at 388, 480 and 650 nm, respectively (Fig. S8A and S12A). The TAS band at 388 nm corresponds to the triplet ^{3}2, 6-AQDS*, whereas the species at 480 and 650 nm correspond to two adducts formed by reaction of the triplet with water.[5] After 1 μs, the absorption around 388 and 650 nm decreased sharply (Fig. S8A), whereas the band centered at 480 nm remained strong (Fig. S8B and S11A). We also found that the 480 nm TAS peak hardly changed in O_2 saturated aqueous solution, indicating that the reaction of ^{3}2, 6-AQDS* with H_2O was much faster than the quenching of ^{3}2, 6-AQDS* by O_2. (Figure S8 C and D) Indeed, reported femtosecond (fs)-TAS studies of related molecules revealed that the generation of the peaks centered at 480 nm and 650 nm started upon 10 ps after laser pulse, with continuous blue shift of the 388 nm peak as it slowly decays, and a continuous red shift of the 480 nm peak.[6]

The kinetic analysis of the absorption of the triplet at 360-410 nm and the adduct at 460-520 nm reveals transient lifetimes (τ) of 0.60 μs and 7.70 μs (Fig. S8E, S8F, and S12C, respectively), although with problem of absorption spectral overlap (Fig. S12A, 2, 6-AQDS).[7, 8] The adduct from 600 nm exhibited short-lived lifetime. Harriman et al. first observed triplet of 2, 6-AQDS in aqueous solution with an analogous spectrum to that reported here and with a lifetime of 1 μs. The formed adduct at 460-520 nm (with lifetime ca. 5 μs) was suggested to be 2, 6-AQDSOH$^-$ transient.[9]

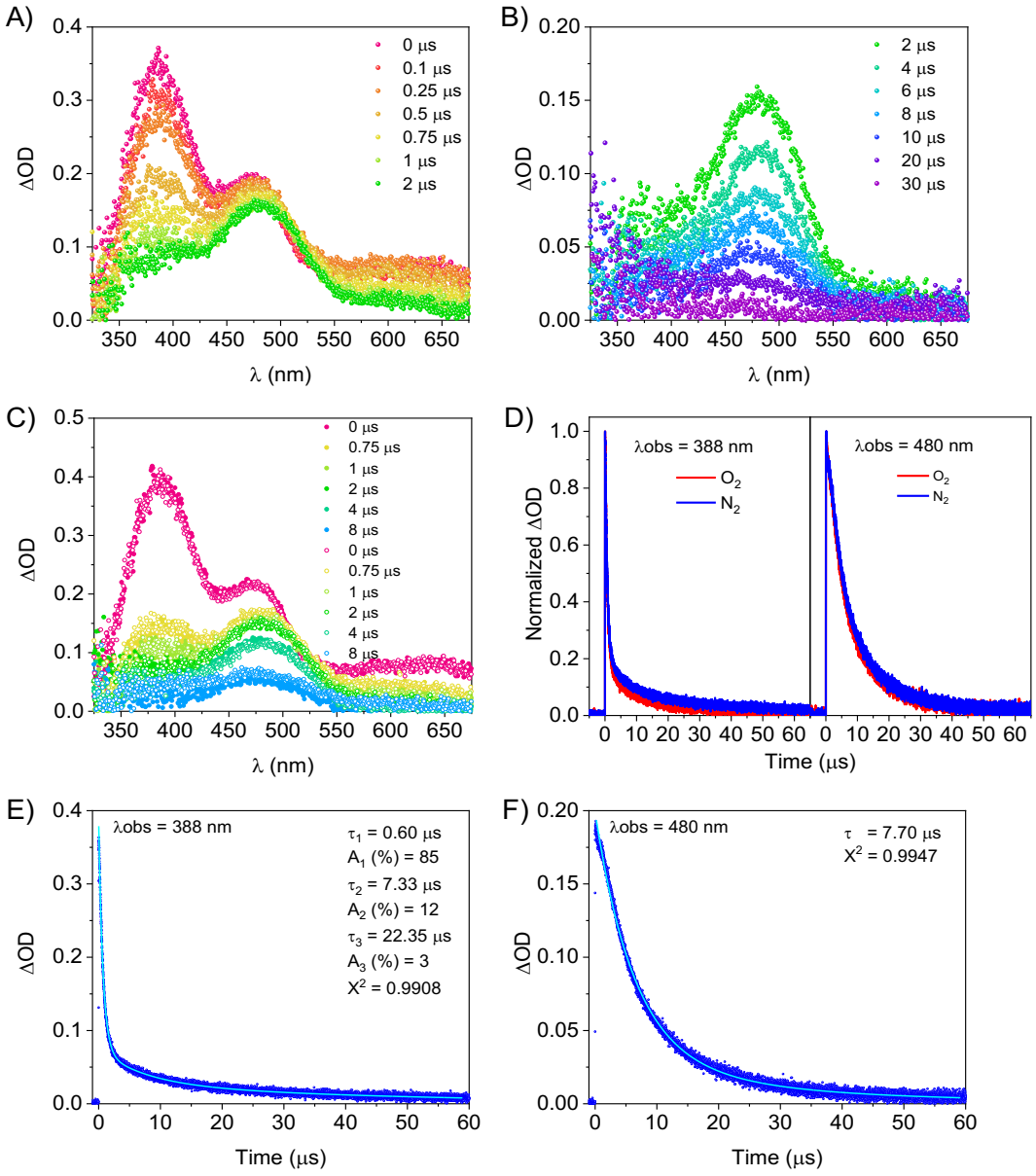

Fig. S8 A and B) Transient absorption spectra (λ_{exc} = 355 nm) for **2, 6-AQDS** ligand in deaerated aqueous solution at different timescales. C) Comparison of transient absorption spectra (λ_{exc} = 355 nm) for **2, 6-AQDS** ligand by the absence (open) or presence (solid) of O_2 in aqueous solution at different timescales. D) Corresponding normalized transient decay traces (λ_{exc} = 355 nm) monitored at λ_{obs} = 388 nm (left) or λ_{obs} = 480 nm (right), respectively, for **2, 6-AQDS** ligand by the absence (blue) or presence (red) of O_2. E and F) Transient decay traces (λ_{exc} = 355 nm) for **2, 6-AQDS** ligand monitored at (C) λ_{obs} = 388 nm or (D) λ_{obs} = 480 nm, respectively. The fitting curves (blue) have been included in all cases.

TAS Experiments of BiPF-10 and BiFePF-15 in Water. For BiPF-10 and BiFePF-15 MOFs, analogous TAS spectra were observed compared the naked linker immediately after laser pulse (Fig. S9A, S10A, and S12A). Interestingly, in both MOFs, a more intense absorption band for 480 nm was noticed upon 0.5 μs (Fig. S9A and S10A) and BiFePF-15 exhibited a broad absorption in all spectral range (Fig. S10A and S10B). In addition, comparing the TAS spectra after 30 μs, the differences become more evident (Fig. S12A). Thus, while 2, 6-AQDS seems inactive, BiPF-10 and BiFePF-15 remained photoactive. These differences were clearly monitored measuring the τ at 480 nm (Fig. S9D, S10D, S11, and S12C). For both MOFs, a remarkable enhancement of τ was observed (11.85 and 19.20 μs for BiPF-10 and BiFePF-15, respectively), confirming a slow-down of the electron-hole pair recombination process.

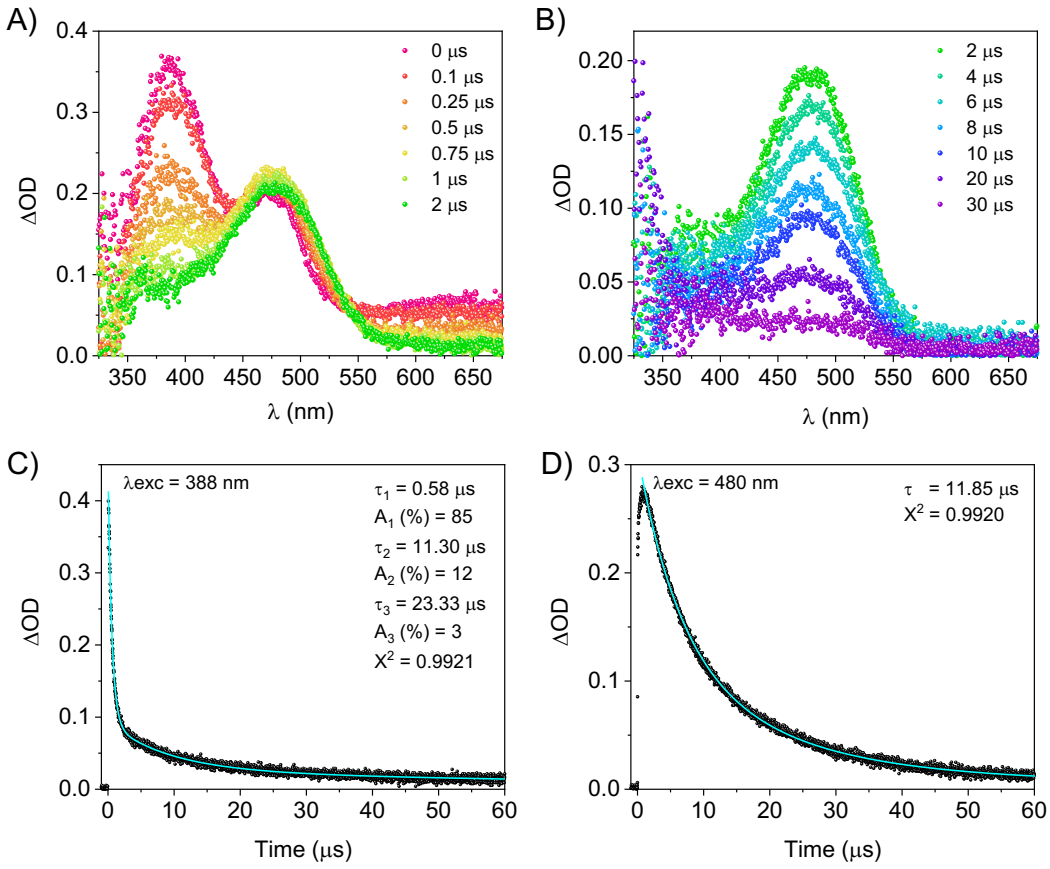

Fig. S9 A and B) Transient absorption spectra (λ_{exc} = 355 nm) for **BiPF-10** MOFs in aqueous solution suspension at different timescales under N_2. C and D) Transient decay traces (λ_{exc} = 355 nm) for **BiPF-10** MOFs monitored at (C) λ_{mon} = 388 nm or (D) λ_{mon} = 480 nm, respectively. The fitting curves (blue) have been included in all cases.

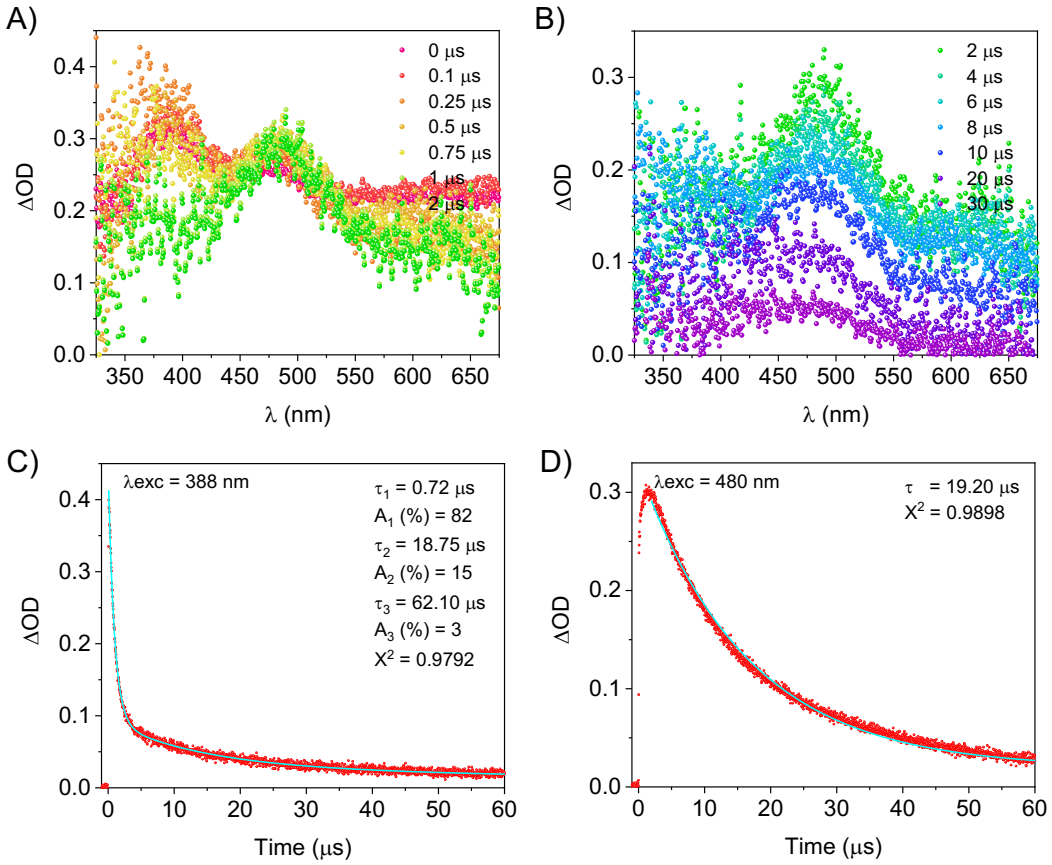

Fig. S10 A and B) Transient absorption spectra (λ_{exc} = 355 nm) for **BiFePF-15** MOFs in aqueous solution suspension at different timescales under N_2. C and D) Transient decay traces (λ_{exc} = 355 nm) for **BiFePF-15** MOFs monitored at (C) λ_{mon} = 388 nm or (D) λ_{mon} = 480 nm, respectively. The fitting curves (blue) have been included in all cases.

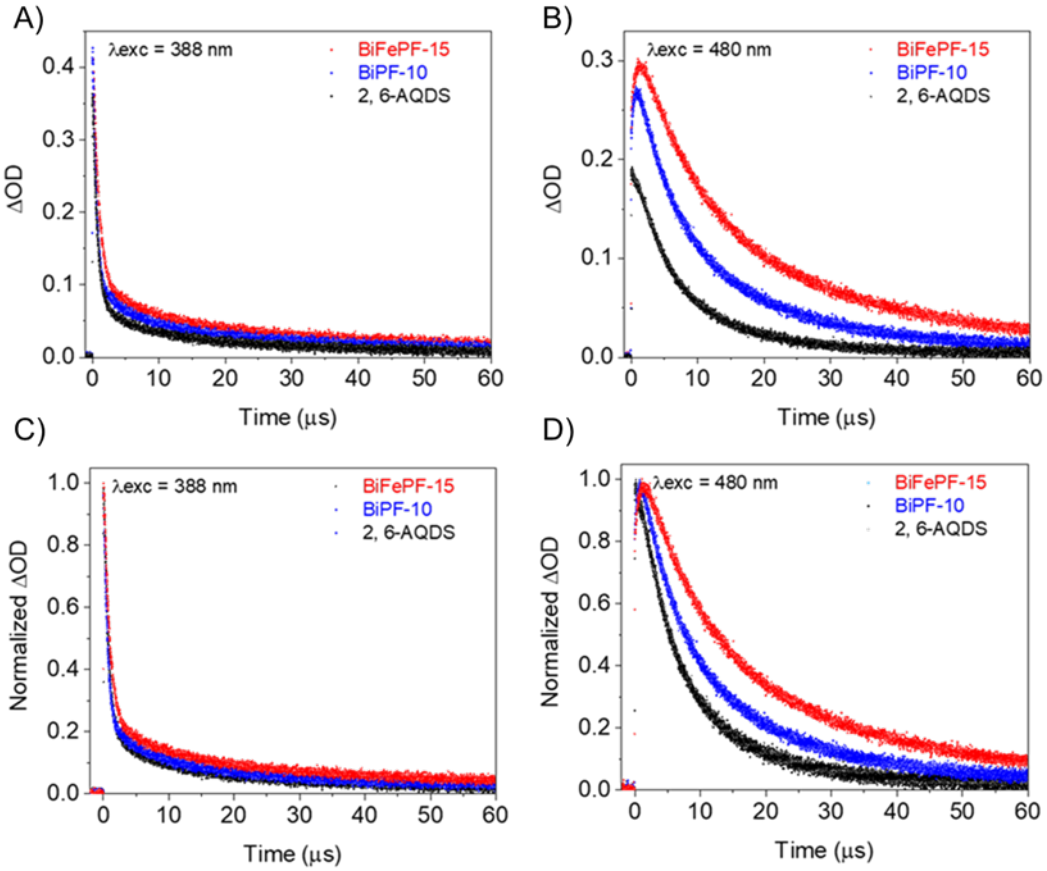

Fig. S11 Comparative of the transient decay traces (A and B) and normalized (C and D) after laser excitation at λ_{exc} = 355 nm for **2, 6-AQDS** ligand and **BiPF-10** and **BiFePF-15** MOFs aqueous samples under N_2 monitored at (A and C) λ_{mon} = 388 nm or (B and D) λ_{mon} = 480 nm, respectively.

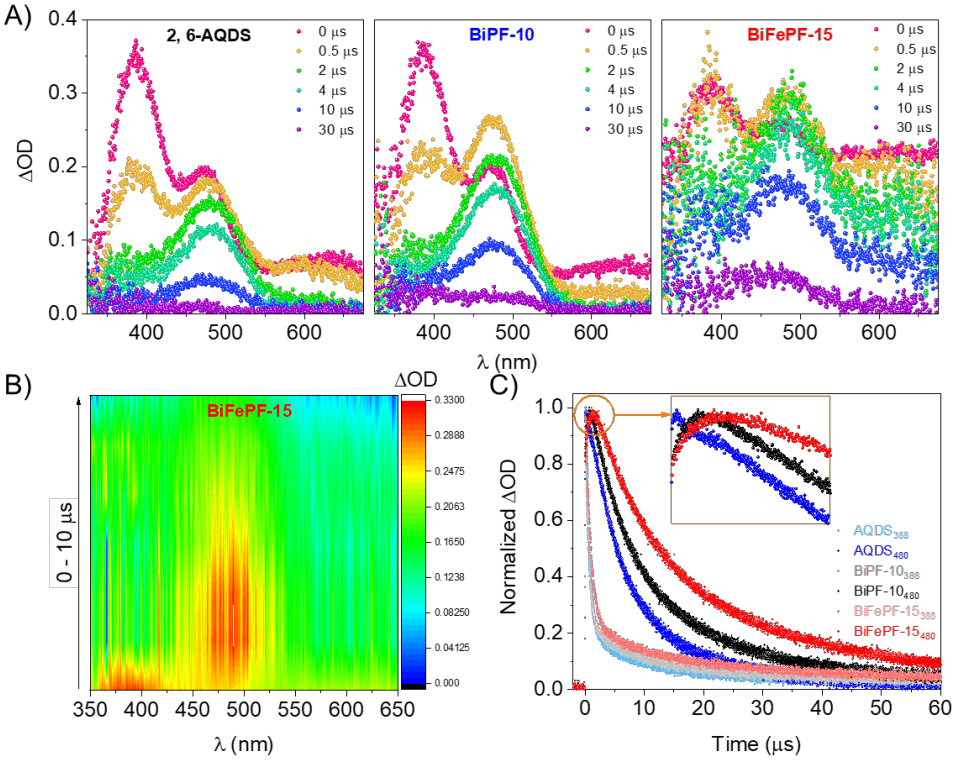

Fig. S12 A) Transient absorption spectra (λ_{exc} = 355 nm) at different timescales and C) comparative of the normalized transient decay traces after laser excitation at λ_{exc} = 355 nm (λ_{mon} = 388 and 480 nm) for **2, 6-AQDS**, **BiPF-10**, and **BiFePF-15** in water under N_2. B) 2D mapping transient absorption spectra of BiFePF-15 in water under N_2.

TAS Experiments of 2, 6-AQDS in the presence of Na_2SO_3. First, in the presence of a high concentration of strong reducing agent (as sodium nitrite or OH^-), the semiquinone radical anion (2, 6-AQDS$^{\bullet-}$) is reported to be produced by electron transfer, which protonates under acidic conditions to produce the neutral radical (2, 6-AQDS$^{\bullet}$).[10] The radical anions produced on AQ possess moderate reduction potentials in their ground states (e.g., E^0(Aq/Aq$^{\bullet-}$) and E^0(Aq-OH/Aq-OH$^{\bullet-}$) are –0.82 and –0.55 V *vs.* saturated calomel electrode (SCE), respectively) and can be accessed electrochemically, chemically, or through photoinduced single-electron transfer (SET) processes in the presence of a suitable electron donor under an inert atmosphere. In general, AQ and its derivatives form colored radical anions upon single-electron reduction. Eggins as well as Lund and Eriksen showed that the excited states of the colored radical anions of AQ are powerful reductants and can be used for photocatalytic reductive transformations.[11, 12]

In our case, we observe transient absorption peaks between 350-425 nm (with maximum at 385 nm) and 450-550 nm (with maximum at 520 nm) and weak absorption at wavelengths >700 nm (Fig. S13A-B, S14A-B, S15A-B, S17). These characteristic bands are consistent with previously reported anion radical 2, 6-AQDS$^{\bullet-}$ (and other AQ derivatives).[13-15] Radical anion 2, 6-AQDS$^{\bullet-}$ exhibited a longer τ of 70-80 μs under inert atmosphere (Fig. S13C and S13D). Owing to the strong overlap of the remained triplet (at 388 nm) and the radical anion absorption bands (385 and 520 nm, respectively), an accurate triplet lifetime was difficult to found. Moore *et al.* defined a quenching rate constant for the triplet state by nitrite of 1.4×10^9 M^{-1} s^{-1}, involving a strong deactivation of triplets by reductive agents.[16] Studies through fs-TAS by Lewis *et al*. demonstrated that the AQ radical anions are formed within 1 ps following laser excitation and the generation of the AQ radical anions in aqueous media is preferably that the formation of AQ$\cdots H_2O$ adducts (> 10 ps after pulse).[14, 17]

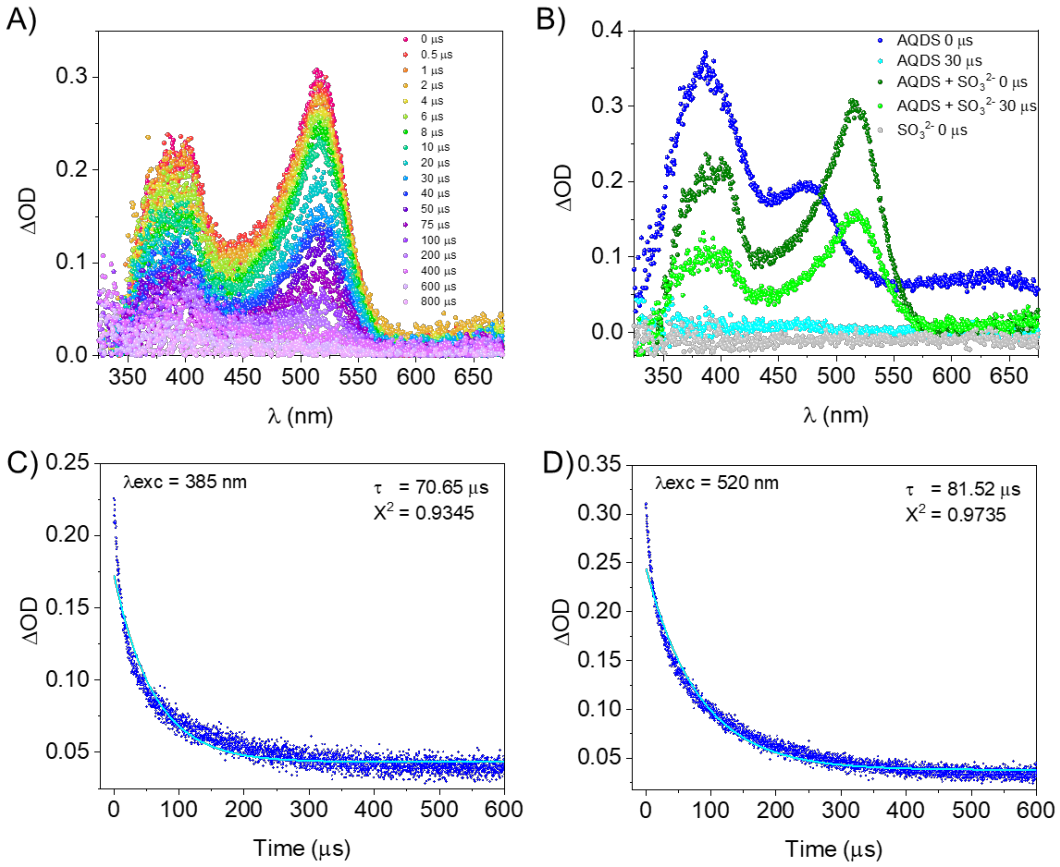

Fig. S13 A) Transient absorption spectra (λ_{exc} = 355 nm) for **2, 6-AQDS** ligand in the presence of 0.5 M Na_2SO_3 in deaerated aqueous solution at different timescales. B) Comparative of the transient absorption spectrum for **2, 6-AQDS** ligand in absence or presence of 0.5 M Na_2SO_3 immediately after laser pulse 0 µs or upon 30 µs. The signal for 0.5 M Na_2SO_3 is included for comparison. C and D) Transient decay traces (λ_{exc} = 355 nm) for **2, 6-AQDS** ligand monitored at (C) λ_{mon} = 385 nm or (D) λ_{mon} = 520 nm, respectively. The fitting curves (blue) have been included in all cases.

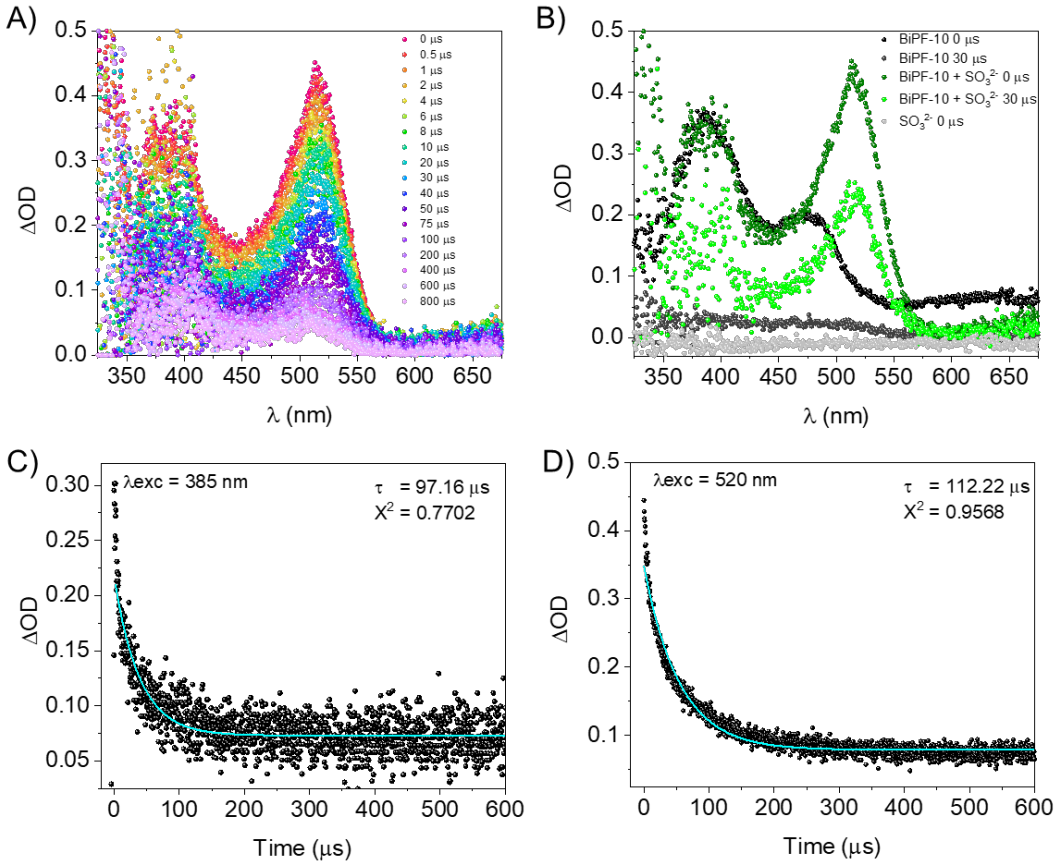

Fig. S14 A) Transient absorption spectra (λ_{exc} = 355 nm) for **BiPF-10** MOFs in the presence of 0.5 M Na_2SO_3 in aqueous solution suspension at different timescales under N_2. B) Comparative of the transient absorption spectrum for **BiPF-10** MOFs in absence or presence of Na_2SO_3 0.5 M immediately after laser pulse 0 µs or upon 30 µs. The signal for 0.5 M Na_2SO_3 is included for comparison. C and D) Transient decay traces (λ_{exc} = 355 nm) for **BiPF-10** MOFs monitored at (C) λ_{mon} = 385 nm or (D) λ_{mon} = 520 nm, respectively. The fitting curves (blue) have been included in all cases.

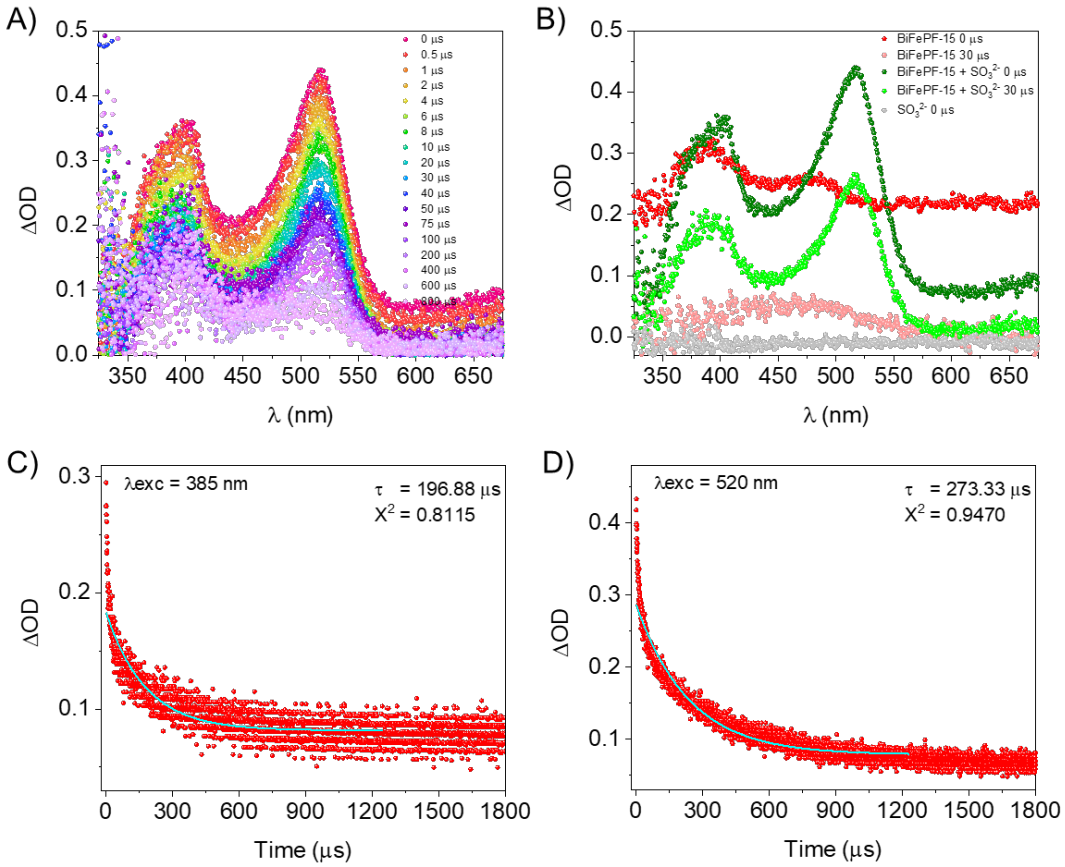

Fig. S15 A) Transient absorption spectra (λ_{exc} = 355 nm) for **BiFePF-15** MOFs in the presence of 0.5 M Na_2SO_3 in aqueous solution suspension at different timescales under N_2. B) Comparative of the transient absorption spectrum for **BiFePF-15** MOF in absence or presence of Na_2SO_3 0.5 M immediately after laser pulse 0 µs or upon 30 µs. The signal for 0.5 M Na_2SO_3 is included for comparison. C and D) Transient decay traces (λ_{exc} = 355 nm) for **BiFePF-15** MOFs monitored at (C) λ_{mon} = 385 nm or (D) λ_{mon} = 520 nm, respectively. The fitting curves (blue) have been included in all cases.

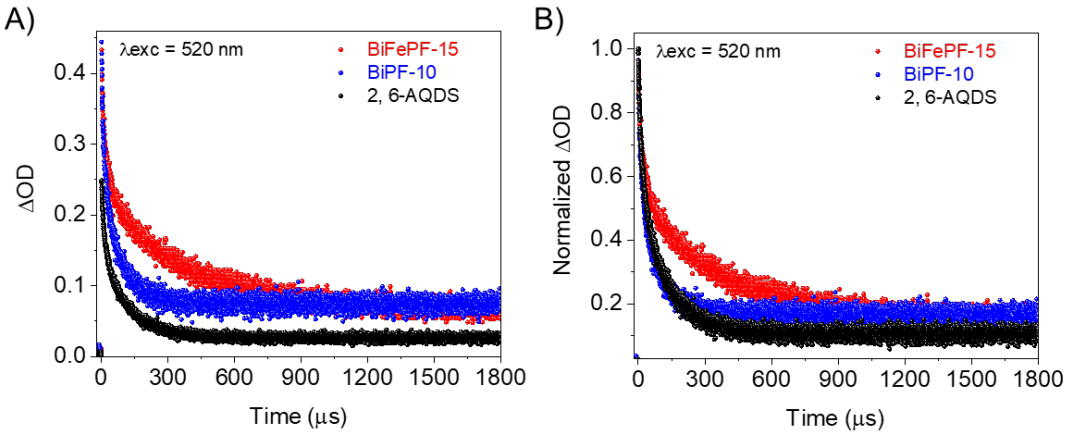

Fig. S16 Comparative of the (A) transient decay traces and (B) normalized after laser excitation at λ_{exc} = 355 nm (λ_{mon} = 520 nm) for **2, 6-AQDS** ligand, **BiPF-10** and **BiFePF-15** MOFs in the presence of aqueous 0.5 M Na_2SO_3 under N_2.

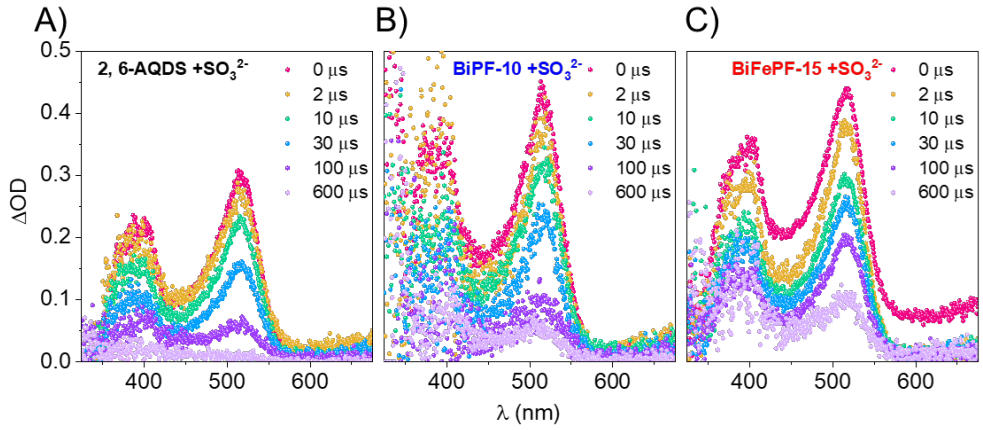

Fig. S17 Comparative transient absorption spectra (λexc = 355 nm) for A) 2, 6-AQDS, B) BiPF-10 and C) BiFePF-15 in the presence of 0.5 M Na_2SO_3 in aqueous solution suspension at different timescales under N_2.

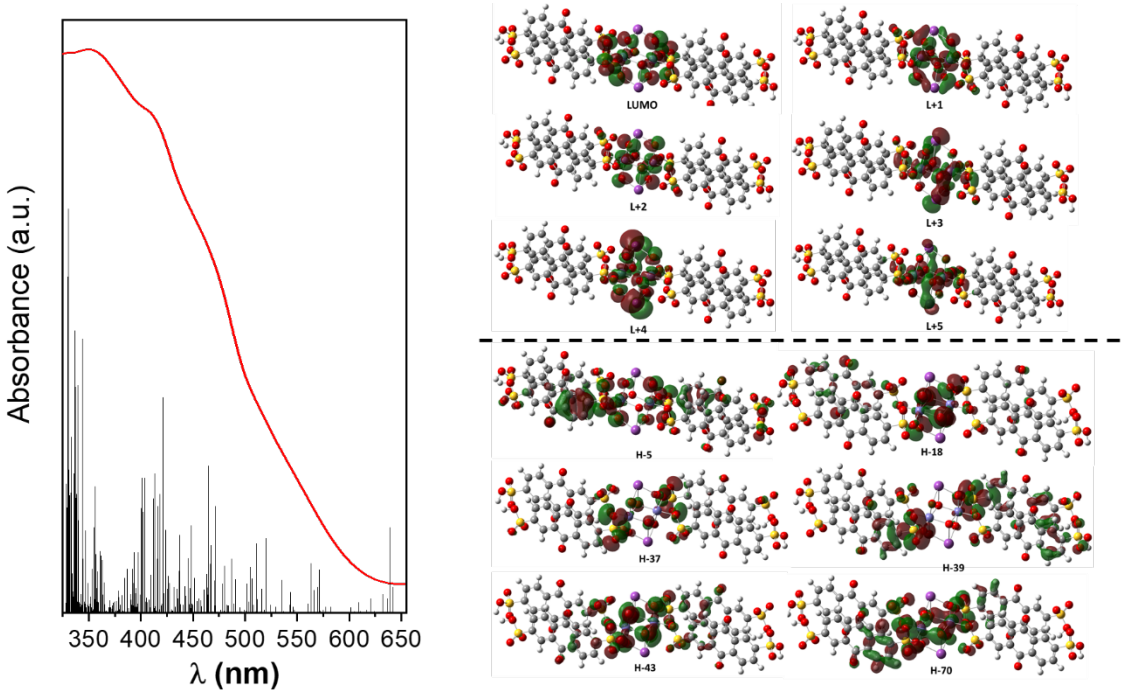

Fig. S18 UV–Vis spectrum of BiFePF-15 and TD-DFT (6-31G**) calculated excitation energies (vertical bars) and selected molecular orbitals contributing to ligand metal charge transfer transitions.

Table S3 Reported bare MOFs used as photo-electrodes for H_2 production.

Catalysts	Light source	Light intensity (mW cm^{-2})	Sacrificial agents	Photosensitizers	Co-catalysts	Applied potential (V *vs.* RHE)	H_2 production rate (μmol h^{-1})	Ref.
MOF-525 (Zr-MOF)	Solar simulator (AM 1.5 solar filter)	100	TEOA	TCPP linker	--	-0.2	0.016	18
IEF-5 (Bi-MOF)	Xe lamp (AM 1.5 solar filter)	253	Na_2SO_3	DTTDC linker	--	1.05	2.35	19
MUV-11 (Ti-MOF)	Solar simulator	253	Na_2SO_3	--	1% Pt	1.2	4.5	20
[La(TTCA)(H_2O)]·DMF·H_2O	High pressure mercury lamp	--	NaOAc/ HOAc	--	--	2.26	1.27 for O_2; 2.48 for H_2	21
Cu_3HHAE_2	Xe lamp (AM 1.5G filter)	100	--	HHAE	--	-0.7	photocurrent density (~260 μA cm^{-2}) at 0V *vs.* RHE	22
BiFePF-15	**Simulated 1 Sun solar simulator (AM 1.5)**	**240**	**Na_2SO_3**	**--**	**--**	**1.0**	**1229.83**	**This work**

References

1 D. Sasikumar, A. T. John, J. Sunny and M. Hariharan, *Chem. Soc. Rev.*, 2020, **49**, 6122-6140.

2 H. J. van Ramesdonk, B. H. Bakker, M. M. Groeneveld, J. W. Verhoeven, B. D. Allen, J. P. Rostron and A. Harriman, *J. Phys. Chem. A*, 2006, **110**, 13145-13150.

3 K. Tickle and F. Wilkinson, Trans. Faraday Soc., 1965, **61**, 1981.

4 A. A. Lamola and G. S. Hammond, *J. Chem. Phys*, 1965, **43**, 2129-2135.

5 S. Goia, M. A. P. Turner, J. M. Woolley, M. D. Horbury, A. J. Borrill, J. J. Tully, S. J. Cobb, M. Staniforth, N. D. M. Hine, A. Burriss, J. V. Macpherson, B. R. Robinson and V. G. Stavros, *Chem. Sci.*, 2022, **13**, 486-496.

6 J. Hankache and O. S. Wenger, *Phys. Chem. Chem. Phys.*, 2012, **14**, 2685-2692.

7 P. R. Maddigapu, A. Bedini, C. Minero, V. Maurino, D. Vione, M. Brigante, G. Mailhot and M. Sarakha, *Photochem. Photobiol. Sci.*, 2010, **9**, 323-330.

8 I. Loeff, A. Treinin and H. Linschitz, *J. Phys. Chem.*, 1983, **87**, 2536-2544.

9 A. Harriman and A. Mills, *Photochem. Photobiol.*, 2008, **33**, 619-625.

10 J. Metcalfe, *J. Chem. Soc. Faraday Trans. 1 Phys. Chem. Condens. Phases*, 1983, **79**, 1721.

11 B. R. Eggins and P. K. J. Robertson, *J. Chem. Soc. Faraday Trans.*, 1994, **90**, 2249.

12 P. Nelleborg, H. Lund and J. Eriksen, *Tetrahedron Lett.*, 1985, **26**, 1773–1776.

13 J. Hankache and O. S. Wenger, *Chem. Commun.*, 2011, **47**, 10145-10147.

14 F. D. Lewis, A. K. Thazhathveetil, T. A. Zeidan, J. Vura-Weis and M. R. Wasielewski, *J. Am. Chem. Soc.*, 2010, **132**, 444-445.

15 A. Mau, W. Sasse, *Aust. J. Chem.*, 1982, **35**, 1723.

16 J. N. Moore, D. Phillips, N. Nakashima and K. Yoshihara, *J. Chem. Soc. Faraday Trans.*, 1986, **82**, 745.

17 R. Carmieli, A. L. Smeigh, S. M. M. Conron, A. K. Thazhathveetil, M. Fuki, Y. Kobori, F. D. Lewis and M. R. Wasielewski, *J. Am. Chem. Soc.*, 2012, **134**, 11251-11260.

18 R. Ifraemov, R. Shimoni, W. H. He, G. M. Peng and I. Hod, *J. Mater. Chem. A*, 2019, **7**, 3046-3053.

19 A. García-Sánchez, M. Gomez-Mendoza, M. Barawi, I. J. Villar-Garcia, M. Liras, F. Gándara and V. A. D. O'Shea, *J. Am. Chem. Soc.*, 2020, **142**, 318-326.

20 N. M. Padial, J. Castells-Gil, N. Almora-Barrios, M. Romero-Angel, I. da Silva, M. Barawi, A. García-Sánchez, V. A. D. O'Shea and C. Martí-Gastaldo, *J. Am. Chem. Soc.*, 2019, **141**, 13124-13133.

21 Y. N. Gong, T. Ouyang, C. T. He and T. B. Lu, *Chem. Sci.*, 2016, **7**, 1070-1075.

22 Y. Lu, H. X. Zhong, J. Li, A. M. Dominic, Y. M. Hu, Z. Gao, Y. L. Jiao, M. J. Wu, H. Y. Qi, C. H. Huang, L. J. Wayment, U. Kaiser, E. Spiecker, I. M. Weidinger, W. Zhang, X. L. Feng and R. H. Dong, *Angew. Chem. Int. Ed.*, 2022, **61**, e202208163.